

## Branching Crisscross Polymerization of Single-Stranded DNA Slats

Jie Deng, Dionis Minev, Anastasia Ershova, and William M. Shih\*

Cite This: *J. Am. Chem. Soc.* 2024, 146, 9216–9223

Read Online

ACCESS |



Metrics &amp; More

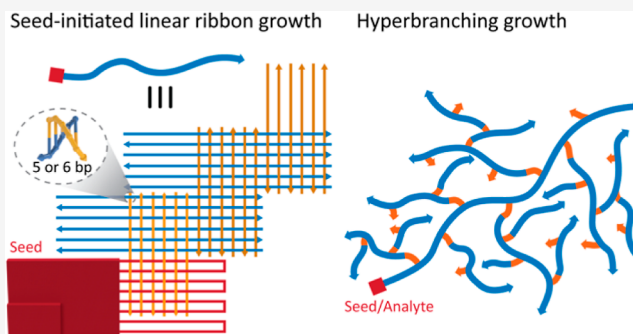


Article Recommendations



Supporting Information

**ABSTRACT:** Controlling where and when self-assembly happens is crucial in both biological and synthetic systems as it optimizes the utilization of available resources. We previously reported strictly seed-initiated linear crisscross polymerization with alternating recruitment of single-stranded DNA slats that are aligned in a parallel versus perpendicular orientation with respect to the double-helical axes. However, for some applications, it would be advantageous to produce growth that is faster than what a linear assembly can provide. Here, we implement crisscross polymerization with alternating sets of six parallel slats versus six perpendicular slats and use this framework to explore branching behavior. We present architectures that, respectively, are designed to exhibit primary, secondary, and hyperbranching growth. Thus, amplification via nonlinear crisscross polymerization can provide a route for applications such as low-cost, enzyme-free, and ultrasensitive detection.



## INTRODUCTION

Nucleation control is a fundamental principle that has been extensively utilized in numerous biological processes, with significant effects on various cellular functions.<sup>1,2</sup> For instance, two major pathways to nucleate actin filaments are the Arp2/3 complex and formin pathways, which play critical roles in dynamic organization of the cytoskeleton and its functions.<sup>3</sup> In synthetic systems, controlling nucleation can be highly valuable for regulating the location and timing of self-assemblies, thus maximizing the efficiency of resource utilization.<sup>4–7</sup> Moreover, the seed for such a system can be encoded with information to guide the trajectory of downstream self-assemblies, e.g., in multifarious assemblies and algorithmic assemblies.<sup>8–11</sup>

Owing to its prominent programmability, DNA has garnered tremendous interest for being used as a building material to fabricate various user-defined structures.<sup>12–15</sup> Most notably, DNA origami with arbitrary 2D and 3D architectures can be fabricated by using one long scaffold strand and multiple short staple strands.<sup>16–18</sup> Controlling nucleation in DNA self-assembly holds particular promise for biomarker detection. In this context, a single target molecule has the potential to trigger the growth of a micro- or macroscale structure, facilitating microscopic or optical readout and enabling ultrasensitive detection methods. Previous studies on nucleation-controlled DNA assemblies, such as DNA bricks and DNA nanotubes assembled from single-stranded DNA (ssDNA) tiles and double-crossover square tiles, respectively, have been extensively explored in terms of structural nanotechnology.<sup>6,7,10,19,20</sup> However, most of these were designed to exhibit linear growth rates, and the demonstration of exponential growth in a seeded structure has been much less

common.<sup>21,22</sup> A key issue is that relatively high rates of spurious nucleation in those systems hinder their further application in diagnosis, although various strategies have been explored for augmenting the energetic barrier for nucleation.<sup>23,24</sup> Alternatively, hybridization chain reactions (HCRs) have been widely used to detect nucleic acid targets, in which the initiator strand (the target) opens the kinetically trapped hairpin strand via toehold-mediated strand displacement.<sup>25–27</sup> However, the HCRs are roughly a hundred to a thousand times slower than hybridization of unimpeded DNA strands.<sup>25,28</sup> Furthermore, it has proven to be challenging to minimize leakage in HCR, especially when implemented in an exponential-amplification format.<sup>29</sup> With proper optimization, HCR systems usually show a limit of detection (LoD) in the picomolar range,<sup>26,27,30,31</sup> which is not sufficient for detection of biomarkers present at only low abundance (e.g., early-stage detection of infectious-disease biomarkers). Hence, there is a growing demand for high-performance, seed-driven exponential signal amplification in enzyme-free systems, ideally with ultralow spurious nucleation coupled to rapid growth, to achieve fast, low-cost, and ultrasensitive biomarker detection.

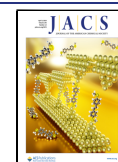
We previously reported the xy-type crisscross polymerization of ssDNA slats (i.e., alternately recruiting x and y slats) through a strictly seeded assembly and have since extended this

Received: January 4, 2024

Revised: March 8, 2024

Accepted: March 11, 2024

Published: March 26, 2024



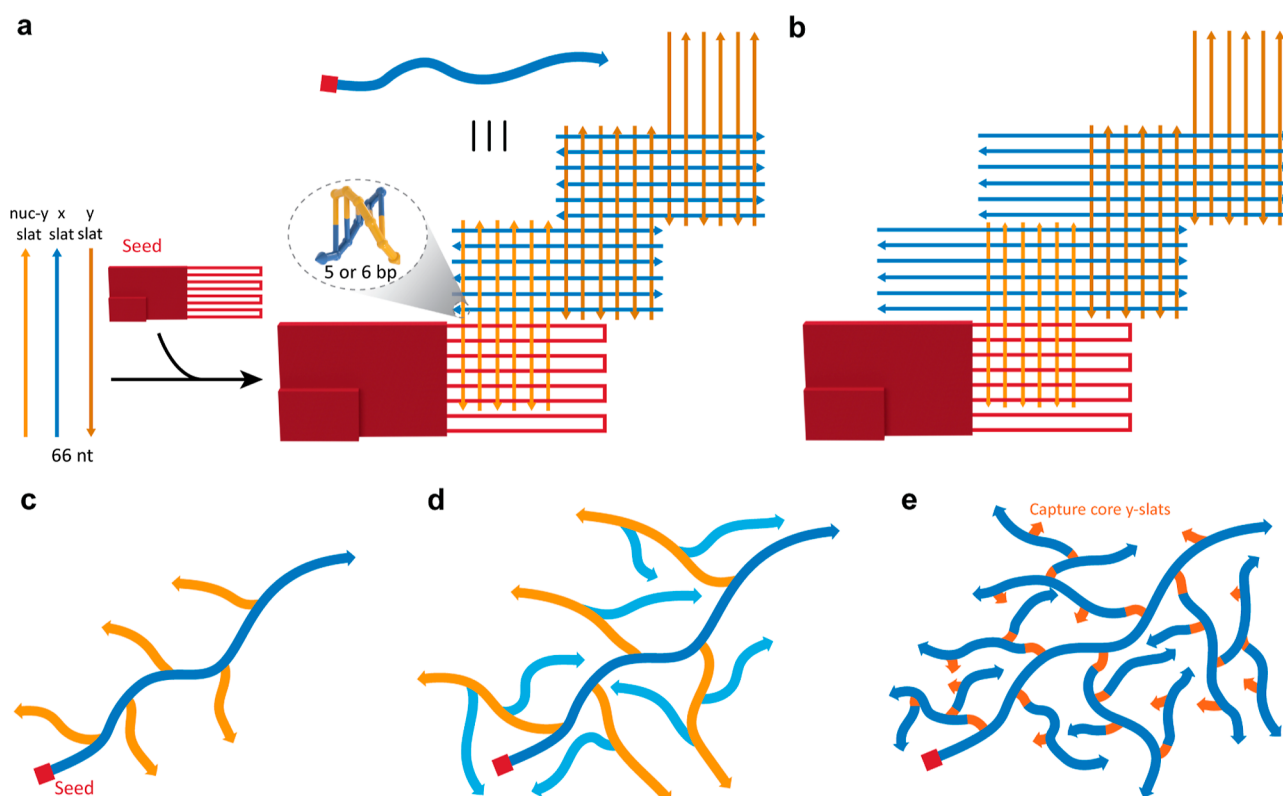


**Figure 1.** Nucleation-controlled zigzag-type crisscross polymerization of ssDNA slats. (a) Schematic illustration for seeded zigzag-type crisscross polymerization of ssDNA slats. The 3' ends of DNA strands are marked with an arrow. Only partial parallel ssDNA arrays from the scaffold strand are depicted in the DNA-origami seed. (b) Same as above but with six-segment x-extensions to enable branching growths. (c–e) Schematic illustrations for (c) primary, (d) secondary, and (e) HypB growth.

method for origami slat assembly for creating multimicron megastructures.<sup>32,33</sup> We believe that ssDNA crisscross assembly offers several features advantageous for biomarker detection, such as a strict nucleation process and fast ribbon growth (i.e., fast signal amplification), with a second-order rate constant of up to  $\sim 10^6 \text{ M}^{-1} \text{ s}^{-1}$ . Critically, one target molecule only leads to one ribbon formation, with an ultimate ribbon length of up to  $\sim 10 \mu\text{m}$ , showing the potential for single-molecule detection. By programming ribbon scission to occur concurrently with growth, we recently expanded isothermal crisscross polymerization from linear to exponential amplification.<sup>34</sup> However, the relatively slow scission limits its application in ultrasensitive detection. An alternative strategy for fast signal amplification would be to implement branching growth such that more growth fronts could be generated on a single-seeded structure, leading to nonlinear signal amplification. Here, we refine our previous design and introduce zigzag-type crisscross polymerization of ssDNA slats (which we previously demonstrated for origami slats<sup>33</sup> and which we describe below), which can better enable branching growth off the extensions elongated from the growth slats. As a result, we realized efficient primary, secondary, and hyperbranching (HypB) growths. Moreover, the growth rate of each individual layer in the branching structures can be adjusted by the slat concentration, providing the ability to tune the morphology of the assembled structures. Unexpectedly, the HypB particles exhibit some degree of splitting into smaller particles, consistent with exponential rather than polynomial growth.

## RESULTS AND DISCUSSION

### General Concept for Nucleation-Controlled Branching Crisscross Polymerization of ssDNA Slats.

In contrast to our previous xy-type crisscross polymerization of ssDNA slats, where each x-slat recruitment follows a prior y-slat recruitment and vice versa,<sup>32</sup> here we applied zigzag-type crisscross polymerization<sup>33</sup> of ssDNA slats, where the growth cycle consists of a series of six y slats that are recruited consecutively, followed by a series of six x slats that are recruited consecutively. A provided DNA-origami seed can bypass the energetic barrier of nucleation via the presentation of a prearranged parallel array of ssDNA segments from the scaffold strand (e.g., M13 bacteriophage-derived “p8064”). Six nuc-y slats can be sequentially recruited by the seed, followed by cycles of addition of six x slats and six y slats for periodic growth of a linear ribbon (Figure 1a). During the assembly, each slat is perpendicularly captured by six binding sites provided coordinately by six ssDNA extensions from the growth front. Each binding site has a length of 5 or 6 nucleotides (nts) (i.e., half-duplex domain), which is defined as one segment on the assembling slat. Each assembling slat consists of six pairs of alternating 5- and 6-nt segments, resulting in 11 base pairs (bp) per turn in the assembled structure. Therefore, a monomer’s half-coordination number is six, giving rise to the term “v6” ribbons.<sup>32</sup> In the absence of a seed, there is a significant energetic barrier to the prearrangement of all six slats into the parallel ssDNA array required for the capture of subsequent slats; in other words, there is a high energetic barrier to undesired spurious nucleation. Hence, the

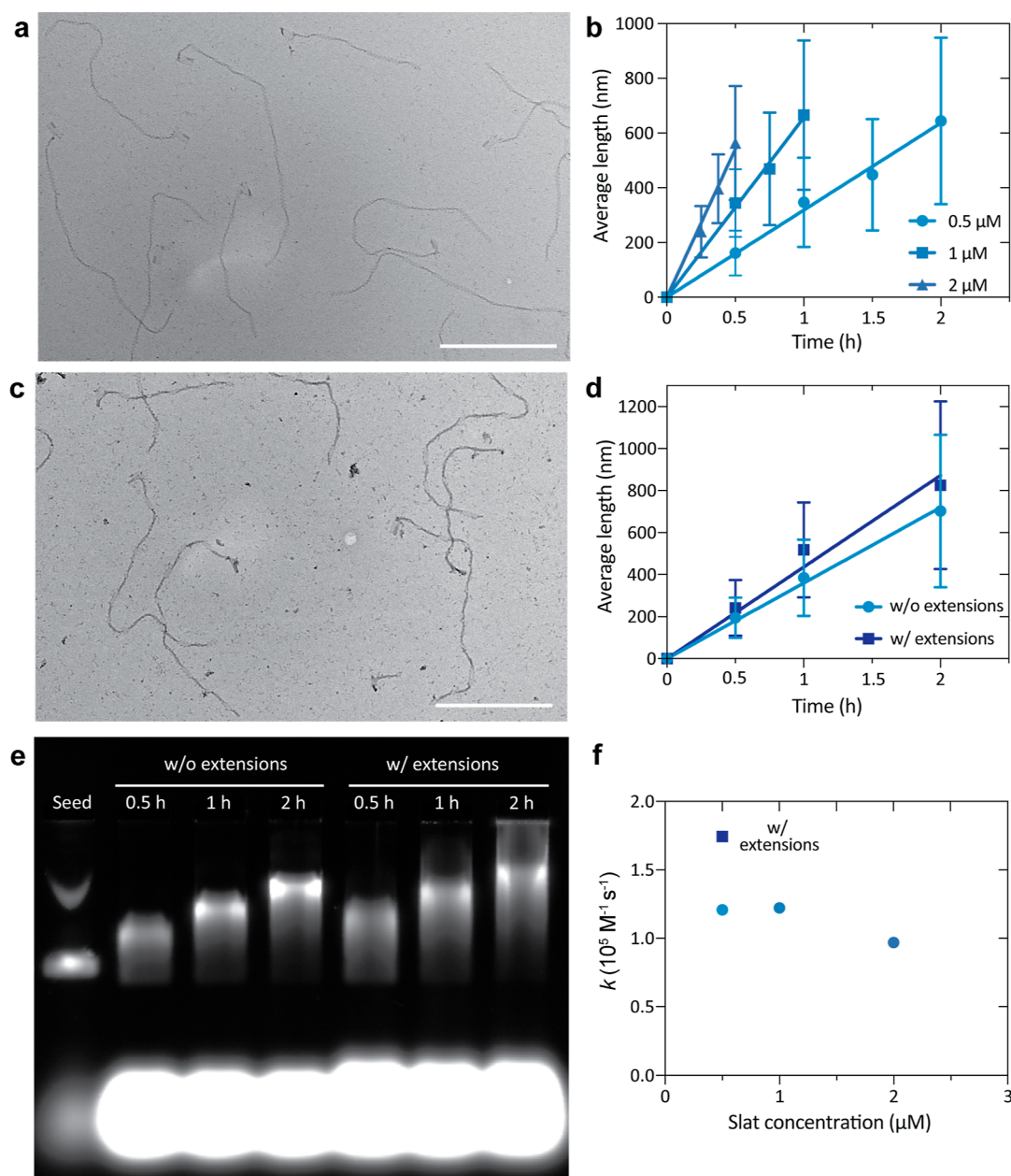


**Figure 2.** Linear zigzag-type crisscross polymerization of ssDNA slats without versus with six-segment x-extensions. (a) TEM image of the assembled ribbons without x-extensions after growth for 2 h. (b) Lengths of the ribbons without x-extensions as a function of time at varied slat concentrations. Error bars correspond to the standard deviation of at least 50 random measurements from multiple fields of view from duplicate experiments. (c) TEM image of the assembled ribbons with x-extensions after growth for 2 h. (d) Lengths of the ribbons without versus with x-extensions as a function of time, using 0.5  $\mu\text{M}$  each assembling slat. Error bars correspond to the standard deviation of at least 50 random measurements from multiple fields of view from duplicate experiments. (e) AGE analyses of the crisscross ribbons as a function of growth time for the systems without versus with x-extensions. (f) Second-order rate constants from fitted lines in (b) and (d) for growths without (circles) versus with (square) x-extensions at different slat concentrations. Scale bars: 500 nm.

crisscross ribbon assembly can manifest as a strictly nucleation-controlled process.

Further elongation of the “core” x slats by six segments allows for primary branching (PriB) growth off the extensions via the recruitment of a set of “primary-branch” nuc-y and periodic “primary-branch” x and y slats (Figure 1a,b). By adding a third layer of crisscross ribbon growth off the y extensions on the primary branches, secondary branching (SecB) growth could be achieved (Figure 1c). Alternatively, HypB growth could be achieved by enabling the recruitment of adapter slats on the x extensions of the core x slats, which in

turn can capture the core y slats (Figures 1d and S1). HypB enables greater signal amplification than PriB or SecB schemes and produces denser particles as output.

**Linear Ribbon Growth without and with x-Extensions.** DNA sequence variation can have a dramatic effect on the growth of crisscross ribbons.<sup>32</sup> Our first step in sequence optimization was to focus on linear zigzag ribbons without x-extensions. We first screened five sequence variants (v6.0–6.4) for linear ribbon growths (see details of sequence design in the Supporting Information and the sequences used in this study in the supporting table), which resulted in three sequence



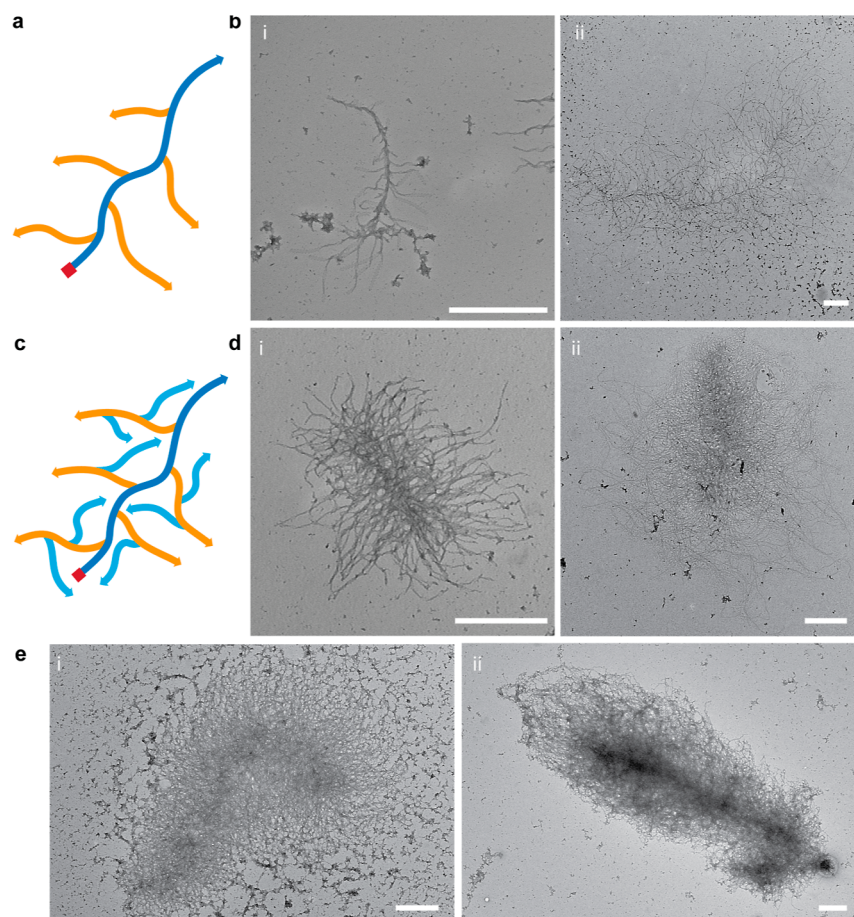


**Figure 3.** PriB and SecB growths. (a) Schematic illustration of PriB growth. (b) TEM images of PriB growth using (i) 100 and (ii) 10 pM seed after 1 and 16 h, respectively. (c) Schematic illustration of SecB growth. (d) TEM images of SecB growth after (i) 4 and (ii) 12 h, using 10 pM seed, 0.2  $\mu\text{M}$  each core slat, 0.25  $\mu\text{M}$  each PriB growth slat, and 0.5  $\mu\text{M}$  each SecB growth slat. (e) TEM images of SecB growth after (i) 4 and (ii) 12 h, using 0.5  $\mu\text{M}$  each slat. Scale bars: 500 nm.

variants performing well (v6.0, v6.3, and v6.4), as observed through agarose gel electrophoresis (AGE) analyses of the final products (Figure S2). Detailed characterization for the growth of linear ribbon was further performed using version 6.0 sequences—which we used exclusively as the “core” for subsequent branching designs—to gain more insights into its assembly kinetics. The experiments were conducted using 1 nM DNA-origami seed and 0.5  $\mu\text{M}$  each nuc-y slat while varying the concentration of the periodic x and y slats, and the growth temperature and  $\text{MgCl}_2$  concentration were optimized at 48  $^\circ\text{C}$  and 16 mM, respectively (Figure S3). The reaction volume for all experiments was standardized to 10  $\mu\text{L}$ , unless otherwise mentioned. Transmission electron microscopy (TEM) (Figure 2a) confirmed the zigzag structure of the ribbon with jagged edges, and the presence of an attached DNA-origami seed on each ribbon was consistent with a nucleation-controlled growth mechanism. For 0.5  $\mu\text{M}$  each periodic assembling slat, the ribbons grow to an average length of  $644 \pm 304.4$  nm after 2 h (Figures 2b and S4), which increases to  $4.5 \pm 2.36$   $\mu\text{m}$  after 16 h (Figure S5). Additionally, the growth rate exhibits linearity with slat concentration when increasing the slat concentration from 0.5 to 2  $\mu\text{M}$  (Figures 2b–f, and S6), manifesting a second-order rate constant of  $1.2 \pm 0.6 \times 10^5 \text{ M}^{-1} \text{ s}^{-1}$ .

To enable branching growth, the x slats were elongated by six segments to the left side of the ribbon (Figure 1b). With

experimentally optimized sequences for the extensions (Figure S7), the growth rate for the linear ribbon with x-extensions could be maintained, with a second-order rate constant of  $1.74 \pm 0.98 \times 10^5 \text{ M}^{-1} \text{ s}^{-1}$  (Figures 2d–f and S8). The ribbons with six-segment extensions on the x slats are highly twisting, as observed by TEM (Figures 2c and S8). Both TEM results and AGE analyses indicate that ribbons with x-extensions grow slightly faster than ribbons without x-extensions (Figure 2e). We speculate that this may be due to undesigned attractive interactions between the x-extensions, which in principle could lead to increased spurious nucleation, but was not observed to be a significant factor for the designs in this present study.

**Primary and Secondary Branching Growths.** Next, we explored PriB growth off the x-extensions (Figure 3a). After systematic optimizations, the primary branch was designed to grow in the southwest direction, given that the core ribbon grows in the northeast direction, and the output domains of the branching nuc-y slats were designed to point in the south direction (Figures S9 and S10). Those criteria also allow for designs that directly use the periodic x- and y-slats from v6.3 and v6.4 sequences for branching growth (versus v6.0 sequences for the core), connected by accordingly modified branching nuc-y slats. The experiments were conducted using 0.1 nM seed and 0.5  $\mu\text{M}$  each core and branching growth slat. TEM images in Figure 3b–i reveal distinct primary branches using v6.4 sequences after growth for 1 h, with a very high

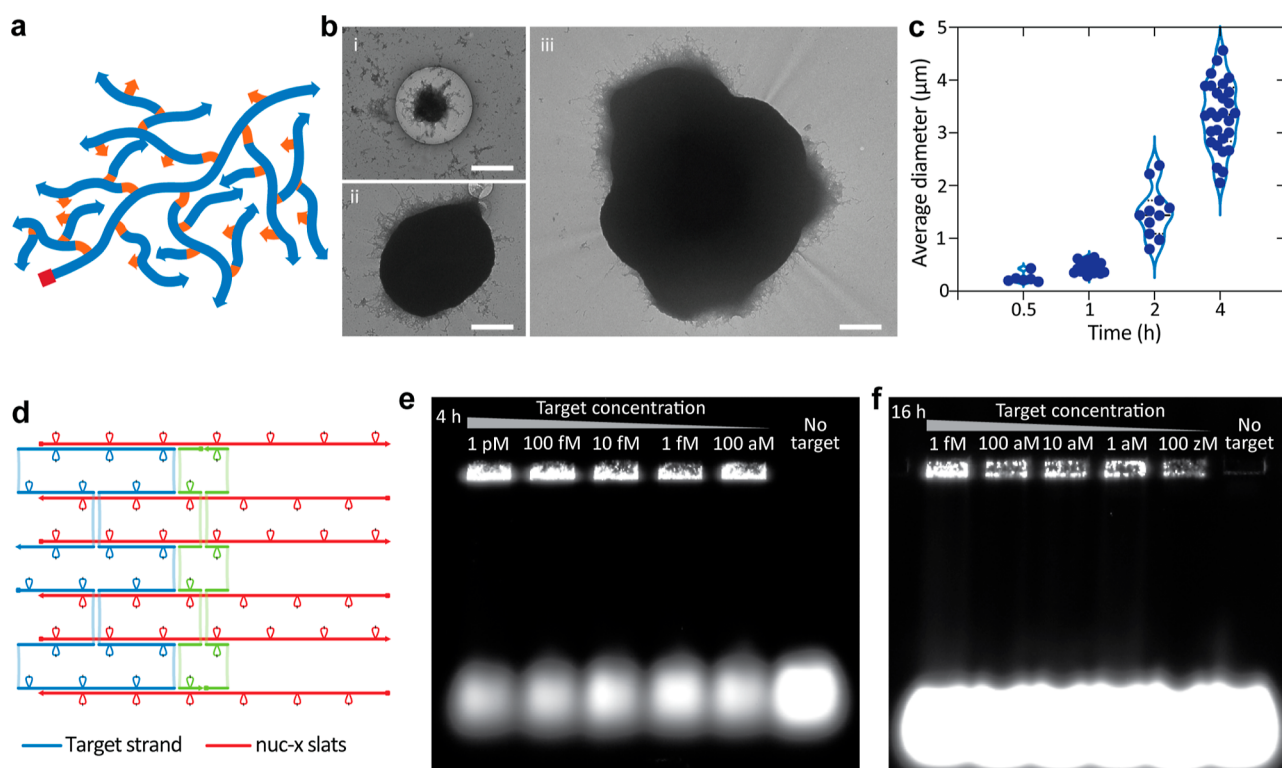


**Figure 4.** HypB growth. (a) Schematic illustration of seeded HypB growth. (b) TEM images for HypB particles after growth for (i) 1, (ii) 2, and (iii) 4 h. (c) Time-dependent diameters of the HypB particles. (d) Designed nanoseed for initiating HypB growth. Two short pre-y slats (green) are included in this design. (e,f) AGE analyses for the seeded HypB growth using varied target concentrations. Scale bars: 500 nm.

branching efficiency. As expected, PriB growth occurs in the opposite direction of core ribbon growth. Due to the highly twisting nature of core ribbons, the primary branches are evenly distributed on both sides of the core ribbon. However, overnight growth does not lead to long primary branches due to a relatively low ratio of branching growth slats per growth front (Figure S10f). Hence, by further decreasing the seed concentration to 10 pM, longer primary branches can be achieved (Figure 3b-ii), and further increasing the concentration of each branching growth slat from 0.5 to 1 μM results in faster branching growth (Figure S11).

To achieve a higher level of structural complexity, a third-layer ribbon growth was appended to the primary branches, resulting in SecB growth (Figure 3c). This process necessitated further sequence optimization in the y-extensions of the primary branches using v6.4 sequences (Figure S12), and the growth follows the same design principles as for PriB growth. The periodic x and y slats from v6.3 sequences were used for the secondary branches. The experiments were initially performed using 1 pM seed, 0.2 μM each core slat, 0.25 μM each PriB growth slat, and 0.5 μM each SecB growth slat. The relatively higher concentration of the SecB growth slats promotes the relative growth rate of the secondary branches, resulting in the formation of hairball-like structures (Figure 3d). When this difference in slat concentration is eliminated and 0.5 μM for each slat is used, growth results in more elongated final structures (Figures 3e and S13). The variation in slat concentration provides a method to tune the assembly kinetics of individual layers, and consequently, the morphology of the structures.

**Hyperbranching Growth and Ultrasensitive Detection of Nucleic Acid Targets.** To further enable even greater

signal amplification of the nucleated structure, for example, to enable ultrasensitive biomarker detection, we explored HypB growth. Figure 4a depicts such a design, in which the seed (red square) nucleates the growth of the core ribbon (blue), and the x-extensions on the core ribbon can recruit six branching nuc-y slats pointing to the south direction, which subsequently can capture six adapter x slats (yellow). The growth front generated by the adapter slats can recapture the input domains of the y-slats for the core ribbon, leading to HypB growth. The growth was first tested using the same origami seed as above. The experiments were performed using 10 fM seed, 0.2 μM each nuc-y slat, 0.5 μM each core ribbon growth slat, and 0.25 μM each branching adapter slat. The reversible temperature for HypB growth under the above conditions was tested to be around 54 °C (Figure S14d). To minimize any possible spurious nucleation, the growth temperature was increased to 50 °C. Time-dependent TEM images provide insights into the kinetics of HypB growth (Figure 4b). After growth for 1, 2, and 4 h, the HypB particles exhibit an average diameter of ca. 0.5, 1.5, and 3.5 μm, respectively (Figures 4b,c and S15), resulting in significantly faster signal amplification than the other types of growths (Figure S14e). A consistent observation throughout our study revealed broken or wrinkled carbon coating in the areas where the particles are situated on the TEM grids. This has led us to speculate that the HypB particles possess a notable rigidity, likely attributed to their dense and alternatingly opposite branching junctions. We propose that the force exerted during the sample preparation, particularly the drying process, exerts a significant impact, causing deformation in the carbon coating surrounding the particles.

We previously demonstrated that crisscross growth could be seeded by a <200 nt target sequence folded into a “nanoseed”



mini-origami.<sup>32,34</sup> Here, we adapted HypB growth to be seeded by a nanoseed (Figures 4d and S16), in which nuc-x slats are used to capture a target strand [either a 198-nt section of M13 p8064 or an ultramer oligonucleotide (IDT)] by five segments from their input domains. The output domains of the nuc-x slats share the same sequences as the output domains of the core x-slats so that the core y-slats can be captured by nuc-x slats to initiate HypB growth. To investigate ultrasensitive detection, we first tested HypB growths with target concentrations varying from 1 pM to 100 aM. The experiments were conducted using 0.1  $\mu$ M each nuc-x slat, 0.25  $\mu$ M each short pre-y slat (green), 0.5  $\mu$ M each core slat, and 0.25  $\mu$ M each branching nuc-y and adapter slat, with a final reaction volume of 10  $\mu$ L and a reaction time of 4 h. AGE analyses of the growths indicate that concentrations as low as 100 aM could be detected (Figures 4e, supplementary S14a–c), as seen by strong stained gel signals for all those HypB growths compared to the negative control, in which no target was added. As the HypB particles quickly grow to a very large size, they cannot migrate into the gel matrix, and the signals in gel pockets are used as the readout to determine positive results, which only provide qualitative, not quantitative, information. Additionally, there is a significant depletion of slat during HypB growth, and a singular particle can persist in its growth even when only one active growth front is present. This underscores a resilient strategy for signal amplification. The ultimate structure is contingent upon the overall quantity of DNA slats employed.

Furthermore, lower ultramer target concentrations were used to check the potential of HypB growth for detecting an ultralow target concentration. The experiments were conducted using 0.1  $\mu$ M each nuc-x slat, 0.125  $\mu$ M each short pre-y slat, 0.25  $\mu$ M each core slat, 0.125  $\mu$ M each branching nuc-y and adapter slat, and varied analyte concentrations ranging from 1 fM to a nominal 100 zM with an order of magnitude decrease per reaction, with a final reaction volume of 20  $\mu$ L, corresponding to an average of 1.2 copies for the lowest concentration. AGE analyses of the growth showed that attomolar concentrations of targets could be detected after growth for 16 h (Figures 4f, S17–S18). This demonstrates the nucleation-controlled growth mechanism for the HypB growth and its specificity to the target analyte.

We note that our initial expectation was for HypB growth, as with any HypB scheme more generally, to display a brief initial exponential phase, followed by a transition to cubic growth due to steric crowding. In practice, however, we observed HypB growth to produce a faster depletion of slats than could be explained by cubic growth, which we attribute to an unexpected self-splitting process (Supplementary Note 1). Additionally, it is worth noting that branching growth can also be achieved via our previous xy-type crisscross growth (Figure S19). However, the xy-type branching growth requires longer extensions and therefore longer strands (i.e., up to 127mers, versus only 99mer longest strands for zigzag growth). Consequently, we ceased exploration of branching growth using xy-type growth. Overall, our results demonstrate that HypB growth is a robust method for rapid signal amplification in an enzyme-free and nucleation-controlled manner.

## CONCLUSIONS

Here, we have introduced nucleation-controlled, branching, zigzag-type crisscross polymerization of ssDNA slats. By implementing PriB, SecB, and HypB growths, we demon-

strated higher levels of structural complexities in ssDNA crisscross assemblies. By varying the concentrations of the core slats and branching slats and, therefore, the relative growth rates of the core and branches, we can tune the morphologies of the branching growth structures. Most strikingly, we have demonstrated rapid structure growth and signal amplification using an architecture designed for HypB, with particles reaching a diameter of several micrometers after 4 h of growth. Our system has the potential for application in ultrasensitive biomarker detection, as demonstrated by our proof-of-concept assay, showing that target concentrations in the attomolar range could be detected after growth for 16 h. In comparison to other single molecule detection technologies, such as droplet digital polymerase chain reaction (PCR),<sup>35,36</sup> quantitative immuno-PCR,<sup>37</sup> single molecule arrays (Simoa),<sup>38,39</sup> digital enzyme-linked immunosorbent assay (ELISA),<sup>40</sup> and fluorescence resonance energy transfer (FRET)-based sensors,<sup>41</sup> our method stands out by eliminating the need for complex instruments like microfluidic devices, qPCR machines, and thermal cyclers. Furthermore, our approach does not rely on enzymes for signal amplification yet achieves comparable detection thresholds (i.e., attomolar), even when employing agarose gel as the readout. This advantage stems from strict nucleation control and rapid crisscross assembly for signal amplification. A current downside of our method is that the rate of amplification remains slow compared to methods such as PCR. The potential for further reduction in detection time exists through DNA sequence optimization or integration with catalytic cascades from other materials. Furthermore, we suggest that multiplexing could be realized through microfluidic chips, chamber devices, or droplet assays. The simplicity and versatility of our method position it favorably for applications demanding efficient and accessible single-molecule detection without the intricacies associated with certain instrumentation and enzymatic processes. We envision that this method, after further development to increase the speed and higher-throughput readout, could be leveraged for low-cost, rapid, and multiplexed biomarker detection from biological samples.

## ASSOCIATED CONTENT

### Supporting Information

The Supporting Information is available free of charge at <https://pubs.acs.org/doi/10.1021/jacs.4c00097>.

Materials; experimental protocols; strand rooting diagram for HypB growth; sequence screening for linear zigzag ribbon growth; screening optimal growth conditions; ribbon length distribution for linear growth; crisscross polymerization of v6.0 ribbon; ribbon growths at varying slat concentrations; extensions optimization for v6.0 ribbon; crisscross polymerization of v6.0 ribbons with six-segment x-extensions; PriB growth with a growth direction perpendicular to the core ribbon; PriB growth with a growth direction opposite to the core ribbon; PriB growths with varied concentrations of branching slats; sequence optimization for the six-segment y-extensions; SecB growth; nanoseed seeded HypB growth; HypB growth; nanoseed designs with varied number of segments for target capturing; HypB growth using a false target strand; amplification of targets diluted to small numbers per well; xy-type

branching growth; and self-splitting in HypB growth-  
(PDF)

Scadnano file for strand rooting diagram of HypB growth off a DNA-origami seed is available at NanoBase (<https://nanobase.org/structure/bd8745db>). Python scripts used to design the sequences for this study are available from the authors upon request.

## AUTHOR INFORMATION

### Corresponding Author

**William M. Shih** — Department of Cancer Biology, Dana-Farber Cancer Institute, Boston, Massachusetts 02215, United States; Wyss Institute for Biologically Inspired Engineering at Harvard University, Boston, Massachusetts 02115, United States; Department of Biological Chemistry and Molecular Pharmacology, Harvard Medical School, Boston, Massachusetts 02115, United States; [orcid.org/0000-0002-1395-9267](https://orcid.org/0000-0002-1395-9267); Email: [William\\_Shih@dfci.harvard.edu](mailto:William_Shih@dfci.harvard.edu)

### Authors

**Jie Deng** — Department of Cancer Biology, Dana-Farber Cancer Institute, Boston, Massachusetts 02215, United States; Wyss Institute for Biologically Inspired Engineering at Harvard University, Boston, Massachusetts 02115, United States; Department of Biological Chemistry and Molecular Pharmacology, Harvard Medical School, Boston, Massachusetts 02115, United States; Present Address: School of Chemistry and Chemical Engineering, Huazhong University of Science and Technology, Wuhan, China; [orcid.org/0000-0001-9774-1240](https://orcid.org/0000-0001-9774-1240)

**Dionis Minev** — Department of Cancer Biology, Dana-Farber Cancer Institute, Boston, Massachusetts 02215, United States; Wyss Institute for Biologically Inspired Engineering at Harvard University, Boston, Massachusetts 02115, United States; Department of Biological Chemistry and Molecular Pharmacology, Harvard Medical School, Boston, Massachusetts 02115, United States; Present Address: CATALOG, Boston, MA 02129, USA.

**Anastasia Ershova** — Department of Cancer Biology, Dana-Farber Cancer Institute, Boston, Massachusetts 02215, United States; Wyss Institute for Biologically Inspired Engineering at Harvard University, Boston, Massachusetts 02115, United States; Department of Biological Chemistry and Molecular Pharmacology, Harvard Medical School, Boston, Massachusetts 02115, United States; [orcid.org/0000-0002-7798-615X](https://orcid.org/0000-0002-7798-615X)

Complete contact information is available at:  
<https://pubs.acs.org/10.1021/jacs.4c00097>

### Notes

The authors declare the following competing financial interest(s): D.M., A.E., and W.M.S. have filed a patent on branching and exponential crisscross amplification (PCT/US2022/050352).

## ACKNOWLEDGMENTS

The authors thank the following funding sources: the Wyss Core Faculty Award, the Wyss Molecular Robotics Initiative Award, and the Alexander S. Onassis Scholarship for Hellenes to A.E.

## REFERENCES

- (1) Wiczkorek, M.; Bechstedt, S.; Chaaban, S.; Brouhard, G. J. Microtubule-associated proteins control the kinetics of microtubule nucleation. *Nat. Cell Biol.* **2015**, *17* (7), 907–916.
- (2) Welch, M. D.; Mullins, R. D. Cellular control of actin nucleation. *Annu. Rev. Cell Dev. Biol.* **2002**, *18* (1), 247–288.
- (3) Pollard, T. D. Regulation of actin filament assembly by Arp2/3 complex and formins. *Annu. Rev. Biophys. Biomol. Struct.* **2007**, *36*, 451–477.
- (4) Jiang, S.; Pal, N.; Hong, F.; Fahmi, N. E.; Hu, H.; Vrbanc, M.; Yan, H.; Walter, N. G.; Liu, Y. Regulating DNA self-assembly dynamics with controlled nucleation. *ACS Nano* **2021**, *15* (3), 5384–5396.
- (5) Hensley, A.; Jacobs, W. M.; Rogers, W. B. Self-assembly of photonic crystals by controlling the nucleation and growth of DNA-coated colloids. *Proc. Natl. Acad. Sci. U.S.A.* **2022**, *119* (1), No. e2114050118.
- (6) Zhang, Y.; Reinhardt, A.; Wang, P.; Song, J.; Ke, Y. Programming the nucleation of DNA brick self-assembly with a seeding strand. *Angew. Chem., Int. Ed.* **2020**, *59* (22), 8594–8600.
- (7) Mohammed, A. M.; Schulman, R. Directing self-assembly of DNA nanotubes using programmable seeds. *Nano Lett.* **2013**, *13* (9), 4006–4013.
- (8) Evans, C. G.; O'Brien, J.; Winfree, E.; Murugan, A. Pattern recognition in the nucleation kinetics of non-equilibrium self-assembly. *Nature* **2024**, *625* (7995), 500–507.
- (9) Murugan, A.; Zeravcic, Z.; Brenner, M. P.; Leibler, S. Multifarious assembly mixtures: Systems allowing retrieval of diverse stored structures. *Proc. Natl. Acad. Sci. U.S.A.* **2015**, *112* (1), 54–59.
- (10) Woods, D.; Doty, D.; Myhrvold, C.; Hui, J.; Zhou, F.; Yin, P.; Winfree, E. Diverse and robust molecular algorithms using reprogrammable DNA self-assembly. *Nature* **2019**, *567* (7748), 366–372.
- (11) Barish, R. D.; Schulman, R.; Rothmund, P. W.; Winfree, E. An information-bearing seed for nucleating algorithmic self-assembly. *Proc. Natl. Acad. Sci. U.S.A.* **2009**, *106* (15), 6054–6059.
- (12) Seeman, N. C. Nucleic acid junctions and lattices. *J. Theor. Biol.* **1982**, *99* (2), 237–247.
- (13) Mao, C.; Sun, W.; Seeman, N. C. Designed two-dimensional DNA Holliday junction arrays visualized by atomic force microscopy. *J. Am. Chem. Soc.* **1999**, *121* (23), 5437–5443.
- (14) Zheng, J.; Birktoft, J. J.; Chen, Y.; Wang, T.; Sha, R.; Constantinou, P. E.; Ginell, S. L.; Mao, C.; Seeman, N. C. From molecular to macroscopic via the rational design of a self-assembled 3D DNA crystal. *Nature* **2009**, *461* (7260), 74–77.
- (15) Ong, L. L.; Hanikel, N.; Yaghi, O. K.; Grun, C.; Strauss, M. T.; Bron, P.; Lai-Kee-Him, J.; Schueder, F.; Wang, B.; Wang, P.; et al. Programmable self-assembly of three-dimensional nanostructures from 10,000 unique components. *Nature* **2017**, *552* (7683), 72–77.
- (16) Rothmund, P. W. Folding DNA to create nanoscale shapes and patterns. *Nature* **2006**, *440* (7082), 297–302.
- (17) Douglas, S. M.; Dietz, H.; Liedl, T.; Högberg, B.; Graf, F.; Shih, W. M. Self-assembly of DNA into nanoscale three-dimensional shapes. *Nature* **2009**, *459* (7245), 414–418.
- (18) Dietz, H.; Douglas, S. M.; Shih, W. M. Folding DNA into twisted and curved nanoscale shapes. *Science* **2009**, *325* (5941), 725–730.
- (19) Mohammed, A.; Velazquez, L.; Chisenhall, A.; Schifffels, D.; Fyngson, D.; Schulman, R. Self-assembly of precisely defined DNA nanotube superstructures using DNA origami seeds. *Nanoscale* **2017**, *9* (2), 522–526.
- (20) Li, W.; Yang, Y.; Jiang, S.; Yan, H.; Liu, Y. Controlled nucleation and growth of DNA tile arrays within prescribed DNA origami frames and their dynamics. *J. Am. Chem. Soc.* **2014**, *136* (10), 3724–3727.
- (21) Schulman, R.; Yurke, B.; Winfree, E. Robust self-replication of combinatorial information via crystal growth and scission. *Proc. Natl. Acad. Sci. U.S.A.* **2012**, *109* (17), 6405–6410.

- (22) He, X.; Sha, R.; Zhuo, R.; Mi, Y.; Chaikin, P. M.; Seeman, N. C. Exponential growth and selection in self-replicating materials from DNA origami rafts. *Nat. Mater.* **2017**, *16* (10), 993–997.
- (23) Sajfutdinow, M.; Jacobs, W. M.; Reinhardt, A.; Schneider, C.; Smith, D. M. Direct observation and rational design of nucleation behavior in addressable self-assembly. *Proc. Natl. Acad. Sci. U.S.A.* **2018**, *115* (26), No. E5877–E5886.
- (24) Chen, H.-L.; Schulman, R.; Goel, A.; Winfree, E. Reducing facet nucleation during algorithmic self-assembly. *Nano Lett.* **2007**, *7* (9), 2913–2919.
- (25) Dirks, R. M.; Pierce, N. A. Triggered amplification by hybridization chain reaction. *Proc. Natl. Acad. Sci. U.S.A.* **2004**, *101* (43), 15275–15278.
- (26) Wei, J.; Gong, X.; Wang, Q.; Pan, M.; Liu, X.; Liu, J.; Xia, F.; Wang, F. Construction of an autonomously concatenated hybridization chain reaction for signal amplification and intracellular imaging. *Chem. Sci.* **2018**, *9* (1), 52–61.
- (27) Lv, W. Y.; Li, C. H.; Li, Y. F.; Zhen, S. J.; Huang, C. Z. Hierarchical hybridization chain reaction for amplified signal output and cascade DNA logic circuits. *Anal. Chem.* **2021**, *93* (7), 3411–3417.
- (28) Ang, Y. S.; Yung, L.-Y. L. Rational design of hybridization chain reaction monomers for robust signal amplification. *Chem. Commun.* **2016**, *52* (22), 4219–4222.
- (29) Yin, P.; Choi, H. M.; Calvert, C. R.; Pierce, N. A. Programming biomolecular self-assembly pathways. *Nature* **2008**, *451* (7176), 318–322.
- (30) Zhao, Y.; Chen, F.; Li, Q.; Wang, L.; Fan, C. Isothermal amplification of nucleic acids. *Chem. Rev.* **2015**, *115* (22), 12491–12545.
- (31) Chai, H.; Cheng, W.; Jin, D.; Miao, P. Recent progress in DNA hybridization chain reaction strategies for amplified biosensing. *ACS Appl. Mater. Interfaces* **2021**, *13* (33), 38931–38946.
- (32) Mineev, D.; Wintersinger, C. M.; Ershova, A.; Shih, W. M. Robust nucleation control via crisscross polymerization of highly coordinated DNA slats. *Nat. Commun.* **2021**, *12* (1), 1741.
- (33) Wintersinger, C. M.; Mineev, D.; Ershova, A.; Sasaki, H. M.; Gowri, G.; Berengut, J. F.; Corea-Dilbert, F. E.; Yin, P.; Shih, W. M. Multi-micron crisscross structures grown from DNA-origami slats. *Nat. Nanotechnol.* **2023**, *18* (3), 281–289.
- (34) Ershova, A.; Mineev, D.; Corea-Dilbert, F. E.; Yu, D.; Deng, J.; Fontana, W.; Shih, W. M. Enzyme-Free Exponential Amplification via Growth and Scission of Crisscross Ribbons from Single-Stranded DNA Components. *J. Am. Chem. Soc.* **2024**, *146* (1), 218–227.
- (35) Schuler, F.; Trotter, M.; Geltman, M.; Schwemmer, F.; Wadle, S.; Domínguez-Garrido, E.; López, M.; Cervera-Acedo, C.; Santibáñez, P.; von Stetten, F.; et al. Digital droplet PCR on disk. *Lab Chip* **2016**, *16* (1), 208–216.
- (36) Yin, J.; Zou, Z.; Yin, F.; Liang, H.; Hu, Z.; Fang, W.; Lv, S.; Zhang, T.; Wang, B.; Mu, Y. A self-priming digital polymerase chain reaction chip for multiplex genetic analysis. *ACS Nano* **2020**, *14* (8), 10385–10393.
- (37) Niemeyer, C. M.; Adler, M.; Wacker, R. Detecting antigens by quantitative immuno-PCR. *Nat. Protoc.* **2007**, *2* (8), 1918–1930.
- (38) Warren, A. D.; Gaylord, S. T.; Ngan, K. C.; Dumont Milutinovic, M.; Kwong, G. A.; Bhatia, S. N.; Walt, D. R. Disease detection by ultrasensitive quantification of microdosed synthetic urinary biomarkers. *J. Am. Chem. Soc.* **2014**, *136* (39), 13709–13714.
- (39) Wu, C.; Garden, P. M.; Walt, D. R. Ultrasensitive detection of attomolar protein concentrations by dropcast single molecule assays. *J. Am. Chem. Soc.* **2020**, *142* (28), 12314–12323.
- (40) Cohen, L.; Cui, N.; Cai, Y.; Garden, P. M.; Li, X.; Weitz, D. A.; Walt, D. R. Single molecule protein detection with attomolar sensitivity using droplet digital enzyme-linked immunosorbent assay. *ACS Nano* **2020**, *14* (8), 9491–9501.
- (41) Gu, Z.; Sun, T.; Guo, Q.; Wang, Y.; Ge, Y.; Gu, H.; Xu, G.; Xu, H. Bead-based multiplexed droplet digital polymerase chain reaction in a single tube using universal sequences: an ultrasensitive, cross-reaction-free, and high-throughput strategy. *ACS Sens.* **2022**, *7* (9), 2759–2766.